Many-Body Dispersion in Model Systems and the Sensitivity of Self-Consistent Screening

Kyle R. Bryenton[1] and Erin R. Johnson[1, 2, a)]
[1)] Department of Physics and Atmospheric Science, Dalhousie University, 6310 Coburg Rd, Halifax, Nova Scotia, B3H 4R2, Canada
[2)] Department of Chemistry, Dalhousie University, 6274 Coburg Rd, Halifax, Nova Scotia, B3H 4R2, Canada

(Dated: 1 May 2023)

ABSTRACT

London dispersion is a weak, attractive, intermolecular force that occurs due to interactions between instantaneous dipole moments. While individual dispersion contributions are small, they are the dominating attractive force between non-polar species and determine many properties of interest. Standard semi-local and hybrid methods in density-functional theory do not account for dispersion contributions, so a correction such as the exchange-hole dipole moment (XDM) or many-body dispersion (MBD) models must be added. Recent literature has discussed the importance of many-body effects on dispersion, and attention has turned to which methods accurately capture them. By studying systems of interacting quantum harmonic oscillators from first principles, we directly compare computed dispersion coefficients and energies from XDM and MBD, and also study the influence of changing oscillator frequency. Additionally, the 3-body energy contributions for both XDM, via the Axilrod-Teller-Muto (ATM) term, and MBD, via a random-phase approximation (RPA) formalism, are calculated and compared. Connections are made to interactions between noble gas atoms, as well as to the methane and benzene dimers, and to two layered materials, graphite and MoS_2. While XDM and MBD give similar results for large separations, some variants of MBD are found to be susceptible to a polarization catastrophe at short range, and the MBD energy calculation is seen to fail in some chemical systems. Additionally, the self-consistent screening formalism used in MBD is shown to be surprisingly sensitive to the choice of input polarizabilities.

1. INTRODUCTION

London dispersion,[1,2] the weakest van der Waals interaction,[3] is an attractive intermolecular force that arises between temporary dipoles of neighbouring atoms. The strength of dispersion interactions depends on factors such as the intermolecular contact area and polarizability. While weaker than ionic, covalent, or hydrogen bonds, London dispersion determines important system properties such as adhesion,[4] friction,[5] surface adsorption,[6] phase-change conditions,[7] stability of supramolecular complexes,[8] packing in molecular crystals,[9] and the shapes of biomolecules[10].

The dispersion interaction between a pair of atoms can be described in terms of a multipole expansion through second-order perturbation theory. The total dispersion energy can then be written as an asymptotic series expansion of the form

$$E_{\mathrm{disp}} = -\frac{C_{6,ij}}{R_{ij}^6} - \frac{C_{8,ij}}{R_{ij}^8} - \frac{C_{10,ij}}{R_{ij}^{10}} - \cdots , \qquad (1)$$

where R_{ij} is the distance between the two atoms i and j, and the C_n's are the so-called dispersion coefficients. C_6 accounts for dipole-dipole interactions, C_8 accounts for dipole-quadrupole interactions, and C_{10} accounts for quadrupole-quadrupole and dipole-octupole interactions.

A number of recent articles have discussed the impact of many-body effects on dispersion interactions and their importance in various chemical or solid-state systems.[11–20] We have argued that many-body effects can be separated into two distinct categories, atomic and electronic, based on the perturbation theory of dispersion.[21] In our definition, atomic many-body effects refer to terms that involve more than two atoms obtained from higher levels of perturbation theory, beyond second order. The most significant of these is the three-body, Axilrod-Teller-Muto (ATM) term[22,23] that arises from third-order perturbation theory. For a trio of atoms, the ATM energy is given by

$$E_{\mathrm{ATM}} = \frac{C_{9,ijk}}{R_{ij}^3 R_{ik}^3 R_{jk}^3} \left[3\cos(\theta_i)\cos(\theta_j)\cos(\theta_k) + 1\right], \qquad (2)$$

where θ_i is the angle between atoms i, j, k with atom i at the vertex. This term predicts repulsion for atoms in equilateral or right-angle triangular configurations, and maximal attraction for linear configurations. Using Dobson's classification of dispersion interactions,[24] these atomic many-body effects can be classified as a subset of the Dobson-B interactions. We have, however, argued that contributions from the ATM term are negligible in molecular systems.[21,25]

Electronic many-body effects refer to the responsiveness of the dispersion coefficients due to the surrounding atoms. The C_n coefficients in Eq. (1) will vary from their free-atom values depending on chemical bonding, atomic charge, coordination, hydrogen bonding, and even the presence of distant atoms or molecules.[21,26] Under Dob-

[a)] Electronic mail: erin.johnson@dal.ca

son's classification, electronic many-body effects account for the entirety of Dobson-A effects and some Dobson-B effects. These electronic many-body effects can cause drastic changes in dispersion coefficients, particularly for inorganic solids.[21,27] Capturing these changes is essential for accurate modelling of a system's dispersion energy, and will be a focus of this work.

Within the context of density-functional theory (DFT), dispersion terms must be explicitly included either through incorporation in the exchange-correlation functional, or through an additive, post self-consistent field (post-SCF) correction. In this work, we will limit our discussion to post-SCF dispersion corrections, of which the exchange-hole dipole moment (XDM)[28–31] and many-body dispersion (MBD)[11,32] methods are two of the most accurate. Both of these models involve dispersion coefficients that respond to changes in atomic environment without introduction of empirical parameters, although the origins of their environment dependence are quite different. MBD is based on a model of interacting harmonic oscillators, while XDM captures changes in dispersion coefficients through use of the self-consistent electron density and its derivatives. There are other essential differences between these two methods, including the form of the dispersion energy, how it is damped for small internuclear separations, whether atomic polarizabilities are treated as isotropic on anisotropic, and whether higher-order terms beyond the leading-order C_6 contribution are taken into account.

While the MBD implementation in FHI-aims computes only the total many-body dispersion energy, it is possible to reformulate the theory in terms of the random-phase approximation (RPA)[33–35] to obtain a decomposition into 2-body, 3-body, and higher-order terms. However, this is very different from the partitioning into electronic (changes in the dispersion coefficients due to the presence of all other atoms in the system) and atomic (ATM and analogous terms from higher orders of perturbation theory) many-body effects described above. For example, in the MBD definition, 3-body terms will include other contributions in addition to the ATM term.[35] Beyond-pairwise terms in MBD have been shown to have large contributions to the overall dispersion energies of molecular crystals,[13] supermolecular complexes,[35] and large biomolecules.[33] Much of the debate in the literature concerning the relative importance of beyond-pairwise dispersion effects is likely due to these disparate definitions.

Given the contrasts between the theoretical underpinnings and mathematical forms of XDM and MBD, it is notable that they give quite comparable accuracy for many common benchmarks for intermolecular interactions, molecular crystals, and layered materials. This has prompted us to take a step back and compare the behaviours of these two dispersion methods for a selection of simple model systems, in which the dispersion physics can be examined in the absence of confusing factors such as choices of electronic structure code, basis set, or exchange-correlation functional.

In this work, we compare XDM and MBD, as well the Tkatchenko-Scheffler (TS) method,[36] on a first-principles interacting quantum harmonic oscillator model at finite separations. Oscillator systems were chosen since they form the basis of the MBD model, while it has been shown that XDM recovers the exact result for the asymptotic interaction between harmonic oscillators from perturbation theory.[21] We consider linear arrangements of two, three, and four oscillators, where a variational model is used to capture changes in the free-oscillator wavefunction due to interactions with its neighbours. Linear arrangements of these small oscillator systems should serve to maximize the magnitude of the ATM term, as well as the polarization anisotropy.[37] The dispersion energy and C_6 coefficients are computed from the variationally optimized wavefunctions with XDM, and compared to the TS and MBD results for the same quantities. The aim is to determine if the methods provide comparable treatment of dispersion, including many-body effects, despite their different theoretical bases. Additionally, calculations are performed on linear chains of noble gas atoms to connect the oscillator results with real atomic systems. Finally, we consider two homo-molecular dimers (methane and benzene) and two layered materials (graphite and MoS_2) to highlight similarities and differences between our model systems and those more relevant to chemistry and materials science.

2. THEORETICAL BACKGROUND

2.1. Overview of DFT

In Kohn-Sham[38,39] DFT, the total energy is written as a functional of the electron density,

$$\rho(\boldsymbol{r}) = \sum_{i=1}^{N} |\psi_i(\boldsymbol{r})|^2 \,, \tag{3}$$

for N electrons occupying orbitals $\psi_i(\boldsymbol{r})$. The DFT energy is

$$E_{\mathrm{DFT}} = T_{\mathrm{KS}} + \int v_{\mathrm{ext}} \rho(\boldsymbol{r}) d\boldsymbol{r} + E_{\mathrm{H}}[\rho] + E_{\mathrm{XC}}[\rho] \,, \tag{4}$$

where the component terms are the Kohn-Sham kinetic energy, T_{KS}, the external potential, v_{ext}, the Hartree energy, E_{H}, and the exchange-correlation energy, E_{XC}. A plethora of forms have been proposed for E_{XC}, resulting in the classification of DFT methods. The most common types used in chemistry and physics applications are the local density approximation (LDA), generalized gradient approximations (GGAs), meta-GGAs, and hybrid functionals.[40,41]

Standard semi-local and hybrid functionals[40–47] do not account for London dispersion forces, so a correction must be added. Here, we will focus on additive, post-SCF dispersion corrections to the DFT energy,

$$E_{\text{total}} = E_{\text{DFT}} + E_{\text{disp}} \,. \tag{5}$$

These corrections are typically based on the second-order perturbation theory of dispersion and examples include the Grimme-D series,[48–52] TS,[11,36] MBD (and its variants),[11,12,32,53–57] and the XDM[28–31] dispersion corrections.

2.2. The Exchange-Hole Dipole Moment Model

The exchange-hole dipole moment (XDM) model[28–31] is a post-SCF, or *a posteriori*, dispersion correction based on second-order perturbation theory. The XDM dispersion energy is calculated via

$$E_{\text{XDM}} = -\sum_i \sum_{j<i} \sum_{n=6,8,10} \frac{f_n^{\text{BJ}}(R_{ij})\, C_{n,ij}^{\text{XDM}}}{R_{ij}^n} \,, \tag{6}$$

which sums over all atom pairs, i and j. This model considers the $n = 6, 8, 10$ terms from the multipole expansion, as it has been shown that the contribution of higher-order terms is negligible.[25] Unlike other dispersion corrections, the foundation of the XDM model is based on the principle that instantaneous dipoles form between reference electrons and their corresponding exchange-correlation holes, approximated simply by their exchange holes. These instantaneous dipoles create dispersion interactions that manifest as attractive forces between atoms.

Eq. (6) uses the Becke-Johnson damping function[28]

$$f_n^{\text{BJ}}(R_{ij}) = \frac{R_{ij}^n}{R_{ij}^n + R_{\text{vdW},ij}^n} \,, \tag{7}$$

where $R_{\text{vdW},ij} = (a_1 R_{c,ij} + a_2)$ is the sum of van der Waals radii, and

$$R_{c,ij} = \frac{1}{3}\left[\left(\frac{C_{8,ij}^{\text{XDM}}}{C_{6,ij}^{\text{XDM}}}\right)^{\frac{1}{2}} + \left(\frac{C_{10,ij}^{\text{XDM}}}{C_{6,ij}^{\text{XDM}}}\right)^{\frac{1}{4}} + \left(\frac{C_{10,ij}^{\text{XDM}}}{C_{8,ij}^{\text{XDM}}}\right)^{\frac{1}{2}}\right] \tag{8}$$

is a "critical" separation for interactions between atoms i and j at which the contributions from the various terms in the multipole expansion become equal. a_1 and a_2 are damping parameters that are fit for use with a particular density functional, and perhaps basis set. Their values are typically determined by minimizing the binding-energy errors for a given benchmark set[58,59] and are kept fixed thereafter.

The exchange-hole dipole moment for a reference electron at point $\boldsymbol{r}_1$ is obtained by integrating the exchange hole over $\boldsymbol{r}_2$ via

$$d_{X\sigma}(\boldsymbol{r}_1) = \int \boldsymbol{r}_2\, h_{X\sigma}(\boldsymbol{r}_1, \boldsymbol{r}_2)\, d\boldsymbol{r}_2 - \boldsymbol{r}_1 \,, \tag{9}$$

where σ is a spin index. Two choices of exchange hole have been used in XDM. In the original version of the model,[28] we used the exact exchange hole

$$d_{X\sigma}(\boldsymbol{r}_1) = \left[\frac{1}{\rho_\sigma(\boldsymbol{r}_1)} \sum_{ij} \psi_{i\sigma}(\boldsymbol{r}_1)\, \psi_{j\sigma}(\boldsymbol{r}_1) \times \int \boldsymbol{r}_2\, \psi_{i\sigma}(\boldsymbol{r}_2)\, \psi_{j\sigma}(\boldsymbol{r}_2)\, d\boldsymbol{r}_2\right] - \boldsymbol{r}_1 \tag{10}$$

and this was shown to give exact C_6 dispersion coefficients for hydrogen and highly accurate results for noble gas atoms.[29] However, for molecules and solids, it was later found to be both more accurate and more efficient to use the Becke-Roussel (BR) exchange hole,[60,61] as it intrinsically captures some correlation effects that serve to localize the full exchange-correlation hole to regions of roughly atomic size. While the BR hole is used in all electronic structure programs that include XDM, we will use the exact exchange hole in the computations on the quantum harmonic oscillators as it is well-suited for this type of system.

To compute accurate dispersion energies for realistic systems, we require the inclusion of higher-order ℓ-pole contributions such as quadrupole ($\ell = 2$) or octupole ($\ell = 3$) moments. If a reference electron is centred at a distance r from its nucleus, the centre of its corresponding exchange hole will be a distance $(r - d_{X\sigma})$ from the nucleus, and so the magnitude of the ℓ-pole moments is then $r^\ell - (r - d_{X\sigma})^\ell$. Thus, the general multipole-moment integral is of the form

$$\langle M_\ell^2 \rangle = \sum_\sigma \int \rho_\sigma(\boldsymbol{r}) \left[r^\ell - (r - d_{X\sigma})^\ell\right]^2 d\boldsymbol{r} \,, \tag{11}$$

and the pairwise $C_{n,ij}$ coefficients for Eq. (6) may be expressed as

$$C_{6,ij}^{\text{XDM}} = \frac{\alpha_i\, \alpha_j \langle M_1^2 \rangle_i \langle M_1^2 \rangle_j}{\alpha_i \langle M_1^2 \rangle_j + \alpha_j \langle M_1^2 \rangle_i} \,, \tag{12}$$

$$C_{8,ij}^{\text{XDM}} = \frac{3}{2} \frac{\alpha_i\, \alpha_j \left(\langle M_1^2 \rangle_i \langle M_2^2 \rangle_j + \langle M_2^2 \rangle_i \langle M_1^2 \rangle_j\right)}{\alpha_i \langle M_1^2 \rangle_j + \alpha_j \langle M_1^2 \rangle_i} \,, \tag{13}$$

$$C_{10,ij}^{\text{XDM}} = 2 \frac{\alpha_i\, \alpha_j \left(\langle M_1^2 \rangle_i \langle M_3^2 \rangle_j + \langle M_3^2 \rangle_i \langle M_1^2 \rangle_j\right)}{\alpha_i \langle M_1^2 \rangle_j + \alpha_j \langle M_1^2 \rangle_i} + \frac{21}{5} \frac{\alpha_i\, \alpha_j \langle M_2^2 \rangle_i \langle M_2^2 \rangle_j}{\alpha_i \langle M_1^2 \rangle_j + \alpha_j \langle M_1^2 \rangle_i} \,. \tag{14}$$

Here, the atomic polarizability, α_i, is approximated as

$$\alpha_i = \alpha_i^{\text{free}} \left(\frac{v_i}{v_i^{\text{free}}} \right), \tag{15}$$

where α^{free} is the free atomic polarizability obtained from readily available reference data,[62] and the effective atomic volume,

$$v_i = \langle r^3 \rangle_i = \sum_\sigma \int r^3 \rho_{i\sigma}(\boldsymbol{r})\, d\boldsymbol{r}\,, \tag{16}$$

for atom i may be expressed in terms of the spin-indexed density, $\rho_{\sigma,i}$, for that atom. We note that XDM treats both the moment integrals and atomic polarizabilities as isotropic, which is not the case in many chemical systems.[35] However, the intermolecular dispersion interactions would be anisotropic as they depend on the specific molecular geometries.

To capture atomic many-body effects, the XDM model may also, optionally, include the 3-body Axilrod-Teller-Muto (ATM) dispersion term,[22,23] defined for XDM as

$$E_{\text{XDM}}^{\text{ATM}} = \sum_{i<j<k} \frac{f_{\text{ATM}}^{\text{BJ}}(R_{ij}, R_{ik}, R_{jk}) C_{9,ijk}^{\text{XDM}}}{R_{ij}^3 R_{jk}^3 R_{ki}^3} \times \left[3\cos(\theta_i)\cos(\theta_j)\cos(\theta_k) + 1\right]. \tag{17}$$

The $C_{9,ijk}$ coefficient arises from the nonadditive instantaneous dipole interactions between atoms i, j, and k, and has the form[25]

$$C_{9,ijk}^{\text{XDM}} = \langle M_1^2 \rangle_i \langle M_1^2 \rangle_j \langle M_1^2 \rangle_k \times \frac{\left[\frac{\langle M_1^2\rangle_i}{\alpha_i^0} + \frac{\langle M_1^2\rangle_j}{\alpha_j^0} + \frac{\langle M_1^2\rangle_k}{\alpha_k^0}\right]}{\left[\frac{\langle M_1^2\rangle_i}{\alpha_i^0} + \frac{\langle M_1^2\rangle_j}{\alpha_j^0}\right]\left[\frac{\langle M_1^2\rangle_i}{\alpha_i^0} + \frac{\langle M_1^2\rangle_k}{\alpha_k^0}\right]\left[\frac{\langle M_1^2\rangle_j}{\alpha_j^0} + \frac{\langle M_1^2\rangle_k}{\alpha_k^0}\right]}. \tag{18}$$

The recommended Becke-Johnson damping function for the ATM term is determined by the product of three f_3^{BJ} damping functions as

$$f_{\text{ATM}}^{\text{BJ}}(R_{ij}, R_{ik}, R_{jk}) = f_3^{\text{BJ}}(R_{ij}) f_3^{\text{BJ}}(R_{ik}) f_3^{\text{BJ}}(R_{jk}). \tag{19}$$

This corrective term to the dispersion energy is omitted from the default implementation of the XDM method as it has been shown to have no effect on the errors in computed binding energies or can even cause the error to slightly increase.[25] It is believed that this behaviour is due to errors from the base density functional being an order of magnitude larger than the ATM dispersion energy for molecular clusters.[31,63]

2.3. The Tkatchenko-Scheffler Model

The Tkatchenko-Scheffler (TS) model[36] only considers the lowest-order dispersion term, corresponding to instantaneous dipole-dipole contributions of the form

$$E_{\text{TS}} = -\frac{1}{2} \sum_{ij} \frac{f_{\text{TS}}^{\text{WY}}(R_{ij})\, C_{6,ij}^{\text{TS}}}{R_{ij}^6}, \tag{20}$$

where the sum is over all electron pairs. $f_{\text{TS}}^{\text{WY}}$ is a Fermi-type Wu-Yang damping function[64] of the general form

$$f^{\text{WY}}(R_{ij}) = \frac{1}{1 + \exp\left[-d\left(\frac{R_{ij}}{\beta R_{ij}^0} - 1\right)\right]}, \tag{21}$$

where d and β are empirical parameters. The TS variant of this damping function has $d = 20$. The effective homoatomic dispersion coefficients ($C_{6,ii}$), static polarizabilities (α_i^0), and vdW radii (R_i^0) may be determined for each atom, i, via

$$C_{6,ii} = C_{6,ii}^{\text{free}} \left(\frac{v_i}{v_i^{\text{free}}}\right)^2, \tag{22}$$

$$\alpha_i^0 = \alpha_i^{\text{free}} \left(\frac{v_i}{v_i^{\text{free}}}\right), \tag{23}$$

$$R_i^0 = R_i^{\text{free}} \left(\frac{v_i}{v_i^{\text{free}}}\right)^{1/3}, \tag{24}$$

where the values of $C_{6,ii}^{\text{free}}$, α_i^{free}, and R_i^{free} are obtained from existing literature tabulations.[65–68] The sum of vdW radii for use in the damping function is $R_{ij}^0 = R_i^0 + R_j^0$. The heteroatomic dispersion coefficients are obtained from their homoatomic counterparts using the Slater-Kirkwood formula:[69–72]

$$C_{6,ij}^{\text{TS}} = \frac{2\alpha_i^0 \alpha_j^0 C_{6,ii} C_{6,jj}}{(\alpha_j^0)^2 C_{6,ii} + (\alpha_i^0)^2 C_{6,jj}}. \tag{25}$$

As with XDM, the atomic polarizabilities and dispersion coefficients are treated as isotropic.

2.4. Self-Consistent Screening Formalism

Through the use of the self-consistent screening (SCS) formalism,[73–75] the polarizabilities may be refined via the SCS equation of classical electrodynamics,

$$\boldsymbol{\alpha}_i^{\text{SCS}}(\mathrm{i}\omega) = \alpha_i^0(\mathrm{i}\omega) + \alpha_i^0(\mathrm{i}\omega) \sum_{j \neq i} \mathbf{T}_{ij}\, \boldsymbol{\alpha}_j^{\text{SCS}}(\mathrm{i}\omega)\,, \tag{26}$$

where $\boldsymbol{\alpha}_i^{\text{SCS}}$ is a tensor that contains the x, y, and z polarizability components for atom i. Eq. (26) may be solved via matrix methods.[53] The initial frequency-dependent polarizability of atom i is approximated using the static

TS polarizability of Eq. (23) by considering the leading term of the Padé series[76–78] as

$$\alpha_i^0(\omega) = \frac{\alpha_i^0}{1-(\omega/\omega_i)^2}\,, \tag{27}$$

where

$$\omega_i = \frac{4}{3}\frac{C_{6,ii}}{(\alpha_i^0)^2} \tag{28}$$

is the characteristic excitation frequency for quantum Drude oscillators, derived from the London dispersion formula.[1]

The second-rank dipole-dipole interaction tensor[72] used in Eq. (26) is given by

$$\mathbf{T}_{ij} = \nabla_{\boldsymbol{R}_i} \otimes \nabla_{\boldsymbol{R}_j} v_{ij}\,, \tag{29}$$

where the interaction potential involves the Gauss error function[79,80] and is

$$v_{ij} = \frac{\mathrm{erf}[R_{ij}/\sigma_{ij}]}{R_{ij}}\,. \tag{30}$$

Here $\sigma_{ij} = \sqrt{(\sigma_i^2+\sigma_j^2)}$ is the effective width of the Gaussian charge distribution for $\sigma_i = (\sqrt{2/\pi}\,\alpha_i^0/3)^{1/3}$. The tensor elements then take the form

$$\begin{aligned}\mathcal{T}_{ij}^{ab} =& \frac{R_{ij}^2\delta_{ab}-3R_{ij}^aR_{ij}^b}{R_{ij}^5}\left[\mathrm{erf}\left(\frac{R_{ij}}{\sigma_{ij}}\right)-\frac{2}{\sqrt{\pi}}\frac{R_{ij}}{\sigma_{ij}}\mathrm{e}^{-\left(\frac{R_{ij}}{\sigma_{ij}}\right)^2}\right]\\ &+\frac{4}{\sqrt{\pi}}\frac{R_{ij}^aR_{ij}^b}{\sigma_{ij}^3R_{ij}^2}\mathrm{e}^{-\left(\frac{R_{ij}}{\sigma_{ij}}\right)^2}\,,\end{aligned} \tag{31}$$

where a and b are Cartesian components $\{x,y,z\}$, and R_{ij}^a denotes the a-component of $\boldsymbol{R}_{ij}$.

Once the SCS polarizability tensors for each atom are obtained via Eq. (26), the mean value of the x, y, and z components, denoted $\alpha_i^{\mathrm{SCS}}(\mathrm{i}\omega)$, may be substituted into the Casimir-Polder integral,[81]

$$C_{6,ij}^{\mathrm{SCS}} = \frac{3}{\pi}\int_0^\infty \alpha_i^{\mathrm{SCS}}(\mathrm{i}\omega)\,\alpha_j^{\mathrm{SCS}}(\mathrm{i}\omega)\,d\omega\,, \tag{32}$$

to obtain the isotropic SCS dispersion coefficients. These C_6 coefficients may then be used in Eq. (20), giving rise to the TS@SCS method. The SCS vdW radii required for the damping function are $R_i^{\mathrm{SCS}} = \left(\alpha_i^{\mathrm{SCS}}/\alpha_i^{\mathrm{free}}\right)^{1/3} R_i^{\mathrm{free}}$, where α_i^{SCS} is the SCS polarizability at zero frequency.

2.5. The Many-Body Dispersion Model

The many-body dispersion model's energy is computed via the coupled fluctuating dipole model (CFDM) Hamiltonian,[82–86] where each atom in the system is represented by a corresponding Drude oscillator[87,88] (i.e. an isotropic quantum harmonic oscillator). The solution of this system requires diagonalizing the $3N\times3N$ $\mathbf{C}^{\mathrm{MBD}}$ matrix, which is composed of 3×3 matrix sub-blocks, $\mathbf{C}_{ij}^{\mathrm{MBD}}$, describing the dipolar coupling between oscillators as

$$\mathbf{C}_{ij}^{\mathrm{MBD}} = \delta_{ij}\left(\omega_i^{\mathrm{SCS}}\right)^2+(1-\delta_{ij})\,\omega_i^{\mathrm{SCS}}\omega_j^{\mathrm{SCS}}\sqrt{\alpha_i^{\mathrm{SCS}}\alpha_j^{\mathrm{SCS}}}\mathbf{T}_{ij}\,, \tag{33}$$

where $\omega_i^{\mathrm{SCS}} = \frac{4}{3}C_{6,ii}^{\mathrm{SCS}}/(\alpha_i^{\mathrm{SCS}})^2$.[89] We note that while Eq. (33) implies the use of SCS, it is not strictly necessary. As only the lowest-order interactions are considered via the dipole-dipole interaction tensor, $\mathbf{T}_{ij}$, MBD is considered a C_6-only method. Although recent work has extended MBD to include quadrupolar terms which would capture C_8 and part of C_{10},[90,91] this so-called MBDQ variant is not presently implemented in any open-source codes to our knowledge. The diagonalization of the $\mathbf{C}^{\mathrm{MBD}}$ matrix yields $3N$ eigenvalues, λ_i, which correspond to the square of the interacting quantum harmonic oscillator frequencies. The MBD interaction energy is then given by the difference of the interacting and non-interacting frequencies as

$$E_{\mathrm{MBD}} = \frac{1}{2}\sum_{i=1}^{3N}\sqrt{\lambda_i}-\frac{3}{2}\sum_{i=1}^{N}\omega_i^{\mathrm{SCS}}\,. \tag{34}$$

The MBD model is based on the adiabatic connection fluctuation-dissipation[92–95] (ACFD) theorem within the random-phase approximation[96,97] (RPA) framework. This ACFD-RPA approach can be used to obtain the correlation energy for a system of N interacting quantum harmonic oscillators for a dipole-dipole interaction potential via[34,53]

$$E_{\mathrm{c,RPA}} = -\frac{1}{2\pi}\int_0^\infty d\omega\sum_{n=2}^{N}\frac{1}{n}\,\mathrm{Tr}\left[(\chi_0 v)^n\right]. \tag{35}$$

Here, χ_0 is the non-interacting response function, and v is the interaction potential. The $\chi_0 v$ term may be written in matrix form as the product $\mathbf{AT}$, where $\mathbf{A}$ is a diagonal $3N\times3N$ matrix with the negative of the frequency-dependent input polarizability for particle i on each of the 3×3 diagonal subblocks, and $\mathbf{T}$ is a dipole-dipole interaction tensor. Eq. (35) enables one to decompose the MBD energy into each of its n-body contributions.

MBD[11] has shown improved performance over the TS[36] model for the S22,[98] S66,[99,100] S66×8,[99–101] and S66×7[32] benchmarks of gas-phase molecular dimers both near and away from their equilibrium geometries.

2.6. Range-Separated Self-Consistent Screening

Tkatchenko *et al.* proposed using a range-separated self-consistent screening variant of MBD, named MBD@rsSCS,[12,32] to damp the dispersion energy at short intermolecular separations. This range separation is accomplished by modifying a Fermi-type damping function,[32] $f_{\mathrm{rsSCS}}^{\mathrm{WY}}$, to damp the dipole-dipole interaction tensor from Eq. (31) into a short-range version, $\mathbf{T}_{\mathrm{SR},ij}$, with elements

$$\mathcal{T}^{ab}_{\mathrm{SR},ij} = \left[1 - f^{\mathrm{WY}}_{\mathrm{rsSCS}}(R_{ij})\right]\mathcal{T}^{ab}_{ij}\,. \tag{36}$$

We note that $f^{\mathrm{WY}}_{\mathrm{rsSCS}}$ has the same form as Eq. (21) but uses $d = 6$, as well as a different β damping parameters from TS, so we have labelled them separately to avoid confusion. The rsSCS polarizabilities, $\alpha_i^{\mathrm{rsSCS}}$, and characteristic excitation frequencies, $\omega_i^{\mathrm{rsSCS}}$, are determined by substitution of $\mathbf{T}_{\mathrm{SR},ij}$ into the SCS equation as given in Eq. (26). Similarly, the long-range dipole-dipole interaction tensor, $\mathbf{T}_{\mathrm{LR},ij}$, is approximated to have a frequency-independent form with elements described by

$$\mathcal{T}^{ab}_{\mathrm{LR},ij} = f^{\mathrm{WY}}_{\mathrm{rsSCS}}(R_{ij})\frac{R^2_{ij}\delta_{ab} - 3R^a_{ij}R^b_{ij}}{R^5_{ij}}\,. \tag{37}$$

Finally, α^{rsSCS}, ω^{rsSCS} and $\mathbf{T}_{\mathrm{LR},ij}$ may be substituted into Eq. (33) to determine the MBD@rsSCS energy, and α^{rsSCS} may be substituted into Eq. (32) to obtain the MBD@rsSCS dispersion coefficients. Extensive benchmarking of MBD@rsSCS has shown slight improvements over MBD across a diverse range of data sets.[13,32,102]

2.7. MBD-Free and MBD-XDM

The MBD model traditionally uses the polarizabilities and C_6 coefficients from the TS model as a starting point for the SCS and rsSCS schemes. However, this choice is rather arbitrary and it is not clear to what extent it impacts the evaluation of the final dispersion coefficients and energies. Here we considered two new variants, which we call MBD-Free and MBD-XDM. These variants are not intended for production use, but rather, to assess the sensitivity of SCS/rsSCS to the starting conditions.

The MBD-Free variant uses a free-atom starting point, allowing us to visualize the effect of SCS separately from the TS model's volume scaling as used in Eqs. (22) and (23). This variant would be expected to be well behaved for systems where a free-atom starting point would be reasonable, such as for noble gas atoms. Conversely, MBD-XDM uses the XDM dispersion model as a starting point. Here, the starting C_6 coefficients and polarizabilities are given by

$$C_{6,ii} = C^{\mathrm{XDM}}_{6,ii}\,, \tag{38}$$

$$\alpha^0_i = \alpha^{\mathrm{free}}_i\sqrt{\frac{C^{\mathrm{XDM}}_{6,ii}}{C^{\mathrm{free}}_{6,ii}}}\,, \tag{39}$$

where the square-root is determined through the comparison of Eqs. (22) and (23). These quantities are then used to evaluate the characteristic excitation frequencies and frequency-dependent polarizabilities that are used as input to the SCS or rsSCS process through Eqs. (27) and (28). The final MBD-Free and MBD-XDM dispersion coefficients are then obtained from the resulting SCS or rsSCS polarizabilties via Eq. (32).

3. INTERACTING OSCILLATOR SYSTEMS

Quantum harmonic oscillators are the classic model system for dispersion. They are at the heart of the MBD method, and XDM has also been shown to be exact for the asymptotic (weakly-interacting) limit for harmonic oscillators.[21] In this work, we aim to model interacting oscillators with XDM over a range of distances and determine if the environment dependence is similar to what is observed for real chemical systems. The ultimate goal will be to compare predicted XDM and MBD energies and dispersion coefficients for harmonic oscillators, and determine if they give equivalent response to surrounding environment/many-body effects.

3.1. The Isotropic Quantum Harmonic Oscillator

To study systems of interacting oscillators we start from the single-oscillator case: the isotropic quantum harmonic oscillator. The corresponding potential has the form

$$V(r) = \frac{1}{2}\,\mu\,\omega^2 r^2\,, \tag{40}$$

where the angular frequency $\omega = \sqrt{k_s/\mu}$ may be written in terms of the effective spring constant, k_s, and reduced mass, μ. The wavefunctions that satisfy the resulting Schrödinger equation are given by[103]

$$\psi_{k\ell m}(r,\theta,\phi) = N_{k\ell}\, r^{\ell} \mathrm{e}^{-\nu r^2} L_k^{\ell+\frac{1}{2}}(2\,\nu\, r^2)\, Y_\ell^m(\theta,\phi)\,, \tag{41}$$

where $N_{k\ell}$ is the normalization constant, $L_k^{(\ell+\frac{1}{2})}(x)$ are the generalized Laguerre polynomials, $Y_\ell^m(\theta,\phi)$ are the spherical harmonic functions, and $\nu = {\mu\,\omega}/{2\hbar}$. The corresponding energy eigenvalues for these wavefunctions are given by

$$E = \hbar\,\omega\left(2k + \ell + \frac{3}{2}\right)\,. \tag{42}$$

The energy is normally described by the single quantum number $n = 2k + \ell$. Here $k \in \mathbb{N}_0$, $\ell \leq n \in \mathbb{N}_0$, and $-\ell \leq m \leq \ell \in \mathbb{Z}$. The wavefunctions in Eq. (41) are square-integrable and normalized over their configuration space $\int_{\mathcal{H}} |\psi_{k\ell m}(\boldsymbol{r})|^2\, d\boldsymbol{r} = 1$, while also satisfying the orthonormality condition for their three quantum numbers: $\langle\psi_{k_1\ell_1 m_1}(\boldsymbol{r})|\psi_{k_2\ell_2 m_2}(\boldsymbol{r})\rangle = \delta_{k_1k_2}\delta_{\ell_1\ell_2}\delta_{m_1m_2}$.

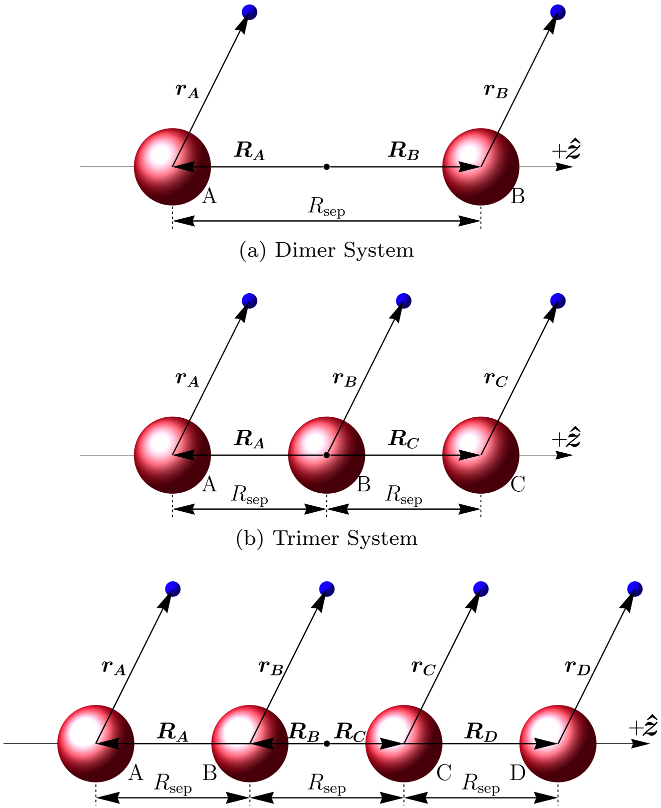

(a) Dimer System

(b) Trimer System

(c) Tetramer System

FIG. 1. The selected geometries for our dimer (a), trimer (b), and tetramer (c) systems of interacting quantum harmonic oscillators, such that all oscillators are aligned along the z-axis. The nucleus of each oscillator is represented by a red sphere, while their corresponding electrons are represented by blue spheres.

3.2. Interaction Hamiltonian

Dimer, trimer, and tetramer systems of interacting oscillators were aligned along the z-axis, as shown in Fig. 1, such that each system is symmetric across the x-y plane. Aligning the oscillators as a linear chain comes with numerous benefits: it reduces the computational resources needed as this first-principles model will scale with $O(N^4)$, linear chains will maximize the polarizability anisotropy captured by the SCS model,[37] and a linear configuration of oscillators will maximize the ATM term.[22] The distance between any two adjacent oscillators is defined as R_{sep}. $\boldsymbol{R}_p$ is the vector that points from the system origin to the nucleus of each oscillator, $p = \{A, B, \ldots\}$, and $\boldsymbol{r}_p$ is the vector that points from the nucleus of oscillator p to its respective electron.

To study the properties of these systems, we first must construct the Hamiltonian which describes them. Within the Born-Oppenheimer approximation,[104] the non-interacting terms (i.e. kinetic and potential energy terms for a single oscillator) in our Hamiltonian have the form

$$\hat{T}_p + \hat{V}_p = -\frac{\hbar^2}{2\mu_p}\nabla_p^2 + \frac{1}{2}\mu_p\omega_p^2 r_p^2\,, \tag{43}$$

for a particular oscillator p. The interactions between the different oscillators will be Coulombic, and will consist of electron-nuclear, electron-electron, and nuclear-nuclear terms. The electron-nuclear term for the electron of oscillator p interacting with the nucleus of oscillator q, with $p \neq q$, is

$$\hat{U}_{pq}^{\text{en}} = \frac{e^2}{4\pi\epsilon_0}\frac{-Z_q}{|(\boldsymbol{R}_p + \boldsymbol{r}_p) - \boldsymbol{R}_q|}\,, \tag{44}$$

where e is the charge of the electron, Z_q is the atomic number of oscillator q, and ϵ_0 is the permittivity of free space. Similarly, the interaction between the electrons of two oscillators p and q is described by

$$\hat{U}_{pq}^{\text{ee}} = \frac{e^2}{4\pi\epsilon_0}\frac{1}{|(\boldsymbol{R}_p + \boldsymbol{r}_p) - (\boldsymbol{R}_q + \boldsymbol{r}_q)|}\,. \tag{45}$$

Lastly, nuclear-nuclear contributions have the form

$$\hat{U}_{pq}^{\text{nn}} = \frac{e^2}{4\pi\epsilon_0}\frac{Z_p\,Z_q}{|\boldsymbol{R}_p - \boldsymbol{R}_q|}\,. \tag{46}$$

Combining these contributions together, the general interaction Hamiltonian is

$$\hat{H} = \sum_p \left(\hat{T}_p + \hat{V}_p\right) + \sum_{q\neq p}\left(\hat{U}_{pq}^{\text{en}} + \frac{1}{2}\hat{U}_{pq}^{\text{ee}} + \frac{1}{2}\hat{U}_{pq}^{\text{nn}}\right)\,. \tag{47}$$

For the electron-nuclear component, the $p = q$ term is omitted because that interaction has been described by the harmonic coupling in Eq. (40). For both the electron-electron and nuclear-nuclear terms, the factor of $1/2$ accounts for the double-counting of contributions.

The systems will be modelled after interacting hydrogen atoms, so we will choose $Z_A = Z_B = 1$. The reduced mass of our system then becomes $\mu = {}^{1836}/{}_{1837}$ a.u. We note that the polarizability of a quantum harmonic oscillator may be expressed in terms of the electron charge, e, and the spring constant, k_s, as $\alpha = e^2/k_s$.[105] Thus, the polarizability and angular frequency are intrinsically linked for this system via

$$\alpha = \frac{e^2}{\omega^2\mu}\,, \tag{48}$$

and choosing $\alpha^{\text{free}} = 4.5$ a.u. to match hydrogen gives a corresponding frequency of $\omega = 0.4715$ a.u. These values were chosen for all calculations unless stated otherwise. Another possible choice is to recall that the first excitation energy for hydrogen is ${}^{3}/{}_{8}$ a.u. and the QHO energy level spacing is $\hbar\omega$. Thus, $\omega = {}^{3}/{}_{8}$ a.u. and $\alpha^{\text{free}} = 7.115$ a.u. is reasonable. Alternatively, the SCS routine selects the characteristic excitation frequency via

Eq. (28). Using $C_{6,ii} = 6.5$ a.u. and $\alpha_i^0 = 4.5$ a.u. to match hydrogen yields $\omega = 0.428$ with a corresponding $\alpha^{\text{free}} = 5.4624$ a.u. The effects on C_6 with these alternate values of ω are discussed in Section 4.3.

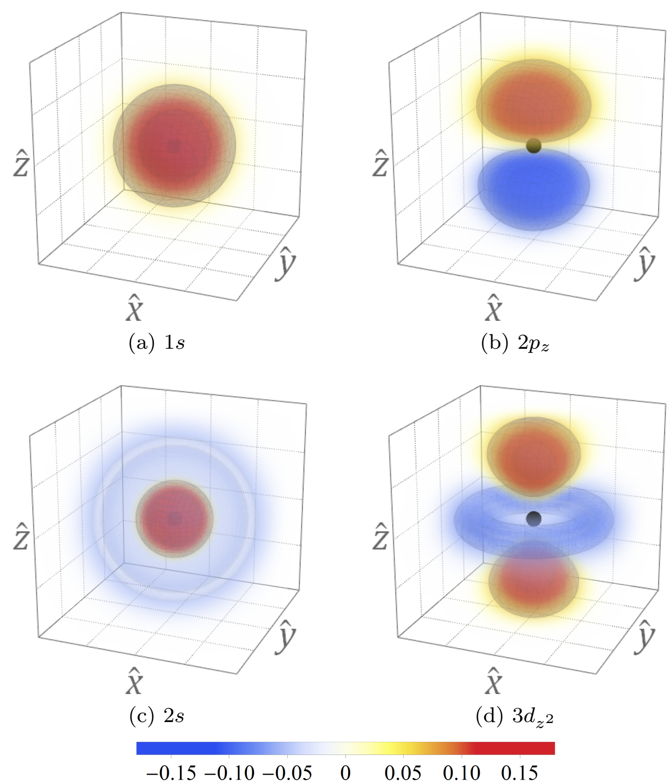

FIG. 2. The $1s$ (a), $2p_z$ (b), $2s$ (c), and $3d_{z^2}$ (d) free-atomic orbitals for the isotropic quantum harmonic oscillator. From the ground, first, and second excited states, these are the only four orbitals that satisfy the bilateral z-axis symmetry requirement for the interacting oscillator chains.

3.3. Wavefunctions

In constructing the wavefunctions for the interacting oscillators, we use the variational method with a basis of hydrogen-like isolated-oscillator wavefunctions. To help connect with chemical intuition, we will refer to these oscillator wavefunctions by their analogous atomic orbital names, determined by their spherical harmonics. Here, we considered wavefunctions from the ground, first, and second excited states that exhibited bilateral symmetry along the z-axis. The only wavefunctions that satisfied this symmetry were the $1s$ orbital from the ground state, the $2p_z$ orbital from the first excited state, and the $2s$ and $3d_{z^2}$ orbitals from the second excited state. Their explicit forms are given by

$$\psi_{1s}(\boldsymbol{r}) = \frac{2^{3/4}\,\nu^{3/4}}{\pi^{3/4}}\,\mathrm{e}^{-\nu r^2} \tag{49}$$

$$\psi_{2p_z}(\boldsymbol{r}) = \frac{2^{7/4}\,\nu^{5/4}}{\pi^{3/4}}\,\mathrm{e}^{-\nu r^2}\,r\cos(\theta) \tag{50}$$

$$\psi_{2s}(\boldsymbol{r}) = \frac{2^{1/4}\,\nu^{3/4}}{\sqrt{3}\,\pi^{3/4}}\,\mathrm{e}^{-\nu r^2}\left(3 - 4\nu r^2\right) \tag{51}$$

$$\psi_{3d_{z^2}}(\boldsymbol{r}) = \frac{2^{3/4}\,\nu^{7/4}}{\sqrt{3}\,\pi^{3/4}}\,\mathrm{e}^{-\nu r^2}\,r^2\left(3\cos(2\theta) + 1\right) \tag{52}$$

and plots of these four orbitals are shown in Fig. 2.

For each oscillator p, the total wavefunction is given as a linear combination of these four orbitals as

$$\Psi_p = \sum_i c_i \psi_{p,i}\,. \tag{53}$$

To ensure symmetry of the wavefunctions across the x-y plane, substitutions of $\theta_p \to \pi - \theta_p$ were made for certain oscillators: θ_B was substituted for the dimer system, θ_C for the trimer system, and both θ_B and θ_D for the tetramer system. These choices permitted constructive orbital overlap between adjacent oscillators allowing us to capture the bonding behaviour of the system. Due to symmetry, the central oscillators (trimer oscillator B, and tetramer oscillators B and C) require different expansion coefficients than the terminal oscillators in each system. The expansion coefficients for the terminal oscillators in each system will simply be written as c_i, while the expansion coefficients for the central oscillators will be written as d_i.

Testing was performed using all 10 wavefunctions from the ground, first, and second excited states on our systems; this confirmed that only the four wavefunctions previously discussed had non-zero contributions. Further testing was performed regarding the inclusion of wavefunctions from the higher energy states, specifically the $3p_z$ and $4f_{z^3}$ orbitals. We determined the inclusion of these orbitals added no additional physics to the system, so they were omitted for computational efficiency.

3.4. Variationally Optimized Energies

From the total wavefunctions, the one-electron energies (i.e. the kinetic, potential, and electron-nuclear terms) are evaluated via

$$E_p^{1\text{e}} = \left\langle \Psi_p \middle| \hat{T}_p + \hat{V}_p + \sum_{q \neq p} \hat{U}_{pq}^{\text{en}} \middle| \Psi_p \right\rangle . \tag{54}$$

The two-electron energies (electron-electron) are similarly computed via

$$E_{pq}^{2\text{e}} = \left\langle \Psi_p \Psi_q \middle| \frac{1}{2} \hat{U}_{pq}^{\text{ee}} \middle| \Psi_p \Psi_q \right\rangle . \tag{55}$$

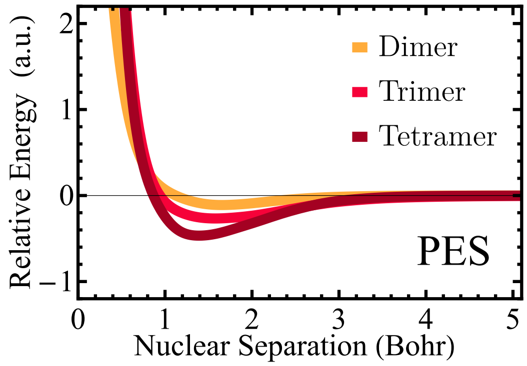

FIG. 3. The computed potential energy surfaces for the interacting quantum harmonic oscillator systems, calculated from first principles using a variational model.

Thus, the total system energy is given by

$$E = \sum_p E_p^{1e} + \sum_{q \neq p} E_{pq}^{2e} + \sum_{q \neq p} \frac{1}{2} \hat{U}_{pq}^{nn} \quad (56)$$

where we note that the nuclear-nuclear terms, $\hat{U}_{pq}^{nn}$, are constant and may be evaluated separately. The optimal values of the expansion coefficients c_i and d_i have yet to be determined. To solve for them, we variationally optimize the wavefunctions using the method of Lagrange multipliers.

The method of Lagrange multipliers will generate the critical points of a multivariate function that is subject to one or more constraint equations.[106] For our oscillator systems, the constraint comes from the normalization requirement of the expansion coefficients, $\sum_i c_i^2 = 1$ and $\sum_i d_i^2 = 1$. The Lagrangian for our singly-constrained dimer system is given by

$$\mathcal{L}(\{c_i\}, \lambda) = E - \lambda \left(1 - \sum_i c_i^2\right), \quad (57)$$

and for the doubly-constrained trimer and tetramer cases,

$$\begin{aligned} &\mathcal{L}(\{c_i\}, \{d_i\}, \lambda_1, \lambda_2) \\ &= E - \lambda_1 \left(1 - \sum_i c_i^2\right) - \lambda_2 \left(1 - \sum_i d_i^2\right), \end{aligned} \quad (58)$$

where the λ are Lagrange multipliers. The critical points on our potential energy surface may be found by solving for the expansion coefficients in the equations generated by $\nabla \mathcal{L} = 0$. The total wavefunctions for our oscillators are determined by substituting these coefficients into the relevant set of wavefunctions in Eq. (53). Thus the coefficients, total wavefunctions, and system energy may been determined for a particular value of R_{sep}. Computing the system energies for a series of separations forms the potential energy surface (PES).

PES for the interacting dimer, trimer, and tetramer systems are shown in Fig. 3. The curves correctly approach the sum of free-oscillator energies in the dissociation limit and give the expected bonding, with the tetramer having the deepest potential energy well, followed by the trimer and dimer. We note that the binding energies are comparable to those of covalent bonds.

3.5. Dispersion Coefficients and Energies for Oscillator Model Systems

From the variationally optimized total wavefunctions, Eq. (3) may be utilized to determine the system's electron density, and a dispersion correction of choice may be used. For all methods described in Section 2, the electron density and the effective volume of Eq. (16) are the starting point. For XDM, the wavefunctions and electron density are used to calculate the exchange-hole multipole moments via Eqs. (10) and (11), which in turn generate the C_n^{XDM} dispersion coefficients and, thus, the XDM dispersion energy. For TS, the effective volumes determine $C_{6,ii}$, α_i^0, and R_i^0 via Eqs. (22) to (24). The $C_{6,ij}^{TS}$ dispersion coefficient is then obtained via the Slater-Kirkwood formula, and the TS dispersion energy follows. From TS and XDM starting points, the SCS or rsSCS polarizabilities can be determined for MBD, MBD-Free, and MBD-XDM, enabling the use of those corrections as well.

4. RESULTS AND DISCUSSION

4.1. Dispersion Energies

We begin by comparing the computed dispersion energies for the harmonic oscillator model systems obtained with the various dispersion methods. Undamped dispersion energies for the interacting dimer, trimer, and tetramer are shown in Fig. 4 for both the XDM and MBD@SCS dispersion models. We additionally show the contribution to the XDM dispersion energy from only the leading-order C_6 dispersion term. The results indicate that the undamped TS, MBD, and C_6-only XDM dispersion energies are in excellent agreement and all three curves are superimposed in the figure. This shows that MBD does not implicitly capture higher-order effects through its self-consistent screening procedure or its model Hamiltonian. It is notable that TS is in agreement with both XDM-C_6 and MBD. This indicates that neither the effects of the exchange-hole dipole for XDM, nor the additional n-body contributions from MBD, are significantly contributing to the dispersion energy for this model system of oscillators.

In previous work using XDM, we established that the C_6 term is responsible for only ca. 60% of the dispersion binding.[28] One may therefore wonder how MBD manages accuracy that rivals that of XDM when neglecting higher-order dispersion terms. To understand this, we

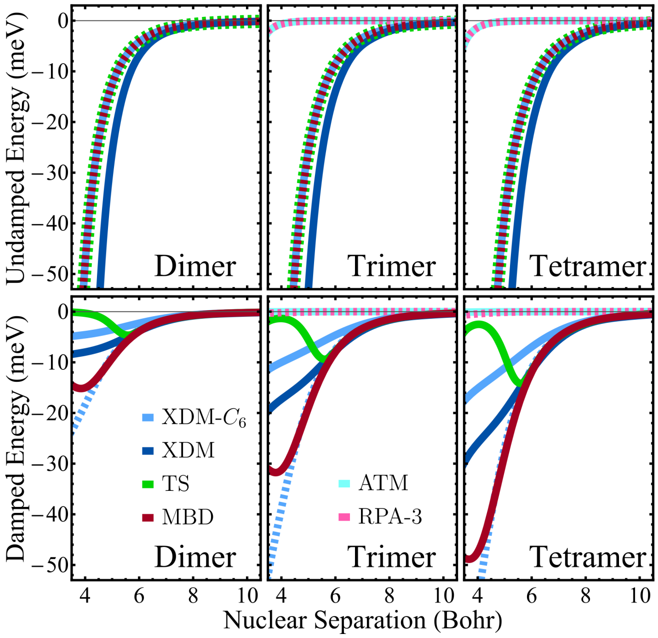

FIG. 4. Computed undamped (top) and damped (bottom) dispersion energies for the harmonic oscillator model systems. The 3-body ATM term was evaluated for XDM but this energy contribution is plotted separately. RPA-3 represents RPA's 3-body-only energy contribution. For the damped XDM-C_6 energies, the typical BJ damping with $a_1 = 0.65$ and $a_2 = 1.68$ Å is shown as a solid line, and with $a_1 = 0$ and $a_2 = 2.30$ Å as a dashed line.

consider the damped dispersion energies, which requires an informed choice of damping parameters.

The damping parameters used in any dispersion model are sensitive to the choice of base DFT method, since they correct in part for errors in the description of non-bonded repulsion provided by the exchange-correlation functional, as well as basis-set incompleteness. To obtain "ideal" damping parameters, we consider the set of six noble-gas dimers consisting of all combinations of He, Ne, and Ar, studied by Kannemann.[107] In that work, the PW86PBE exchange-correlation functional[108,109] with the aug-cc-pV5Z basis set and counterpoise correction[110] was chosen to give as accurate as possible a treatment of non-bonded repulsion to pair with a dispersion correction. The optimal parameters were determined by minimizing the root-mean-square percent error in the binding energies for all six dimers.

The ideal BJ damping parameters for use with XDM were found to be $a_1 = 0.65$ and $a_2 = 1.68$ Å.[107] For the current study, we optimized the β parameter from the Wu-Yang damping function in Eq. (21) for both TS and MBD@rsSCS. Here, the TS and MBD@rsSCS dispersion energies were evaluated with FHI-aims using the PBE functional and "tight" basis sets. The dispersion energies were then combined with the literature PW86PBE/aug-cc-pV5Z counterpoise-corrected electronic energies. This ensured that the damping functions were parameterized in as similar a way as possible to allow direct comparison. The optimal damping parameters for TS and MBD@rsSCS were determined to be $\beta_{\mathrm{TS}} = 0.86$ and $\beta_{\mathrm{rsSCS}} = 0.62$ respectively. Lastly, we wanted to see how TS and MBD@rsSCS compare to XDM-C_6, the C_6-only contribution to the damped XDM energy. Using the same methodology, reparameterizing XDM-C_6 resulted in optimal BJ damping parameters of $a_1 = 0$ and $a_2 = 2.30$ Å, since a_1 must have a non-negative value.

Using these ideal damping parameters, a comparison of the damped dispersion energies from XDM, TS, and MBD is shown in Fig. 4. Interestingly, the MBD, TS, and XDM damped dispersion energies track each other closely at large internuclear separations (>6 Bohr). This is also the case for XDM-C_6 when the BJ damping parameters are optimized for the C_6-only energy, but not when using the full-XDM parameterization. At short range, the TS dispersion energy is strongly damped, while MBD actually provides greater dispersion stabilization than the full XDM dispersion energy, and is in notably high agreement with the reparameterized XDM-C_6 for >4 Bohr. Thus, the choice of damping can cause the MBD dispersion energy to resemble the full XDM dispersion energy rather than only the C_6 term, in the same way that a weaker damping function on XDM-C_6 can achieve similar results.

For the trimer and tetramer, the contributions of both the ATM term and the 3-body energy from RPA are included. The ATM contribution to the energy was calculated with XDM as described in Section 2.2. For the RPA contribution, each of the n-body contributions to the correlation energy were extracted from Eq. (35). We compare these 3-body contributions for undamped and damped trimer and tetramer systems at all computed separations beyond 4 Bohr. To ensure fair comparison between the RPA energy and MBD, the SCS starting point was used for the undamped energies, and rsSCS was used for the damped energies. The individual n-body RPA and MBD energies were compared, and found to be within 1% of each other. Further, the 2-body RPA energy captured no less than 97.9% of the total many-body energy. There is remarkably high agreement between the undamped ATM and 3-body RPA energies, as seen from the nearly superimposed curves in Fig. 4, differing by no more than 3.2%. These results agree with our previous finding[21] that the ATM term represents a negligible contribution to the overall dispersion energy.

4.2. Analysis of C_6 Behaviour

Next, we analyze the changes in C_6 coefficients themselves. The computed C_6 coefficients are plotted in Fig. 5 as a function of internuclear separation for the dimer, trimer, and tetramer models, with separate plots for the symmetry distinct (central and terminal) oscillators. Results are shown for the TS and XDM dispersion models, as well as for the SCS and rsSCS schemes used in

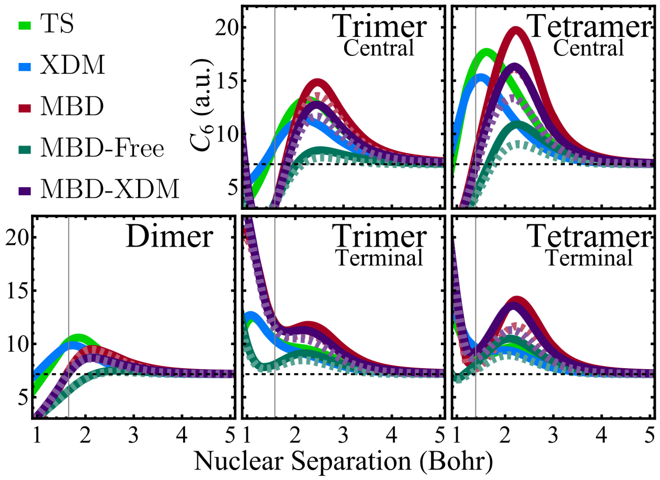

FIG. 5. The analysis of C_6 for the oscillator chains. For the MBD methods, solid lines are C_6 coefficients derived from SCS polarizabilities and dashed lines are derived from rsSCS polarizabilities. The vertical lines indicate the equilibrium bond distances for each system.

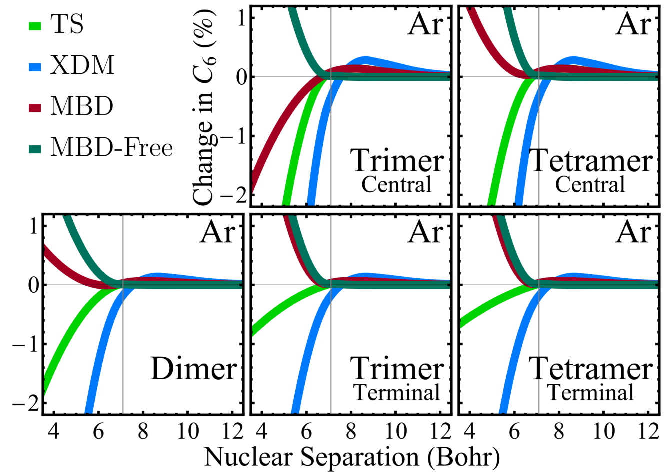

FIG. 6. Variation in C_6 for argon chains, from FHI-aims calculations using the PBE density functional with "tight" basis sets. For the MBD methods, the rsSCS routine was used. The vertical lines indicate the reference equilibrium separation for the Ar dimer.[111]

MBD with the usual TS (MBD), free-atom (MBD-Free), or XDM (MBD-XDM) starting points. While the SCS and rsSCS C_6 coefficients do not explicitly appear in the MBD energy expression, their magnitude is directly related to the dispersion stabilization.

Overall, all of the methods give dispersion coefficients that are responsive to changes in the local environment of each oscillator. The C_6 coefficients all correctly approach the free-oscillator limit at large separations. They then reach a maximum value as the separation decreases to between 2-3 Bohr. While there is some variation depending on the particular model system and internuclear separation, the dispersion coefficients follow the rough trend of MBD $>$ MBD-XDM $>$ TS $>$ XDM $\gg$ MBD-Free. Thus, the SCS and rsSCS schemes are surprisingly sensitive to the choice of starting polarizabilities and dispersion coefficients. This stands in sharp contrast to the usual self-consistent evaluation of DFT energies, which are typically insensitive to the choice of starting guess (provided convergence can be reached). A more subtle trend is that SCS tends to give larger changes in C_6 than rsSCS.

The increase in C_6 (relative to the infinitely separated limit) is smallest for the terminal oscillators, followed by the central oscillator in the trimer and tetramer, with the latter showing the highest C_6 values. This change with environment is captured by all of the models. The C_6 increase between the free oscillators, terminal oscillators, and central oscillators is an example of what we mean by electronic many-body effects and could also be considered Dobson-A effects. Additionally, the higher C_6 for the central oscillators of the tetramer, relative to the trimer, would not be captured by a simple coordination number descriptor.

To connect with the oscillator data, we performed calculations on a similar chemical system: linear argon chains. The geometries were analogous to those shown in Fig. 1, with the separation between each Ar atom held fixed at the same R_{sep}. These calculations were performed with the XDM, TS, and MBD dispersion models, all using the PBE density functional[109] and the "tight" basis sets in the FHI-aims package.[112,113] Here, the PBE functional was chosen because it is the recommended GGA to pair with MBD. As such, PBE was used for all calculations in this study to ensure a fair comparison between dispersion methods, despite the fact that combining XDM with a dispersionless base functional such as B86bPBE[109,114] results in higher accuracy.[47] For these calculations, we also modified the code to implement MBD-Free, which was expected to give similar results to MBD for noble gases where a free-atom reference is highly intuitive. The computed dispersion coefficients for the argon dimer, trimer, and tetramer are shown in Fig. 6, where all MBD methods used the rsSCS routine.

The argon-chain results show that the dependence on surrounding environment is qualitatively similar to that seen for the quantum harmonic oscillators. The XDM, TS, and MBD dispersion coefficients again increase beyond their free-atom values as the internuclear distance is shortened and reach maximum values. However, these maximum values are obtained at much larger separations of roughly 8-9 Bohr, which is reasonable given the larger atomic size and far weaker binding. The maximum C_6 coefficients are again lower for the terminal atoms than the central atoms, although the results are quite similar for the central atoms of the trimer and tetramer, unlike for the oscillators.

At short separations in Fig. 6 (and in some cases in Fig. 5 as well), MBD and MBD-Free's dispersion coefficients show unusual behaviour as they begin to sharply increase. We believe this is a symptom of a "polarization

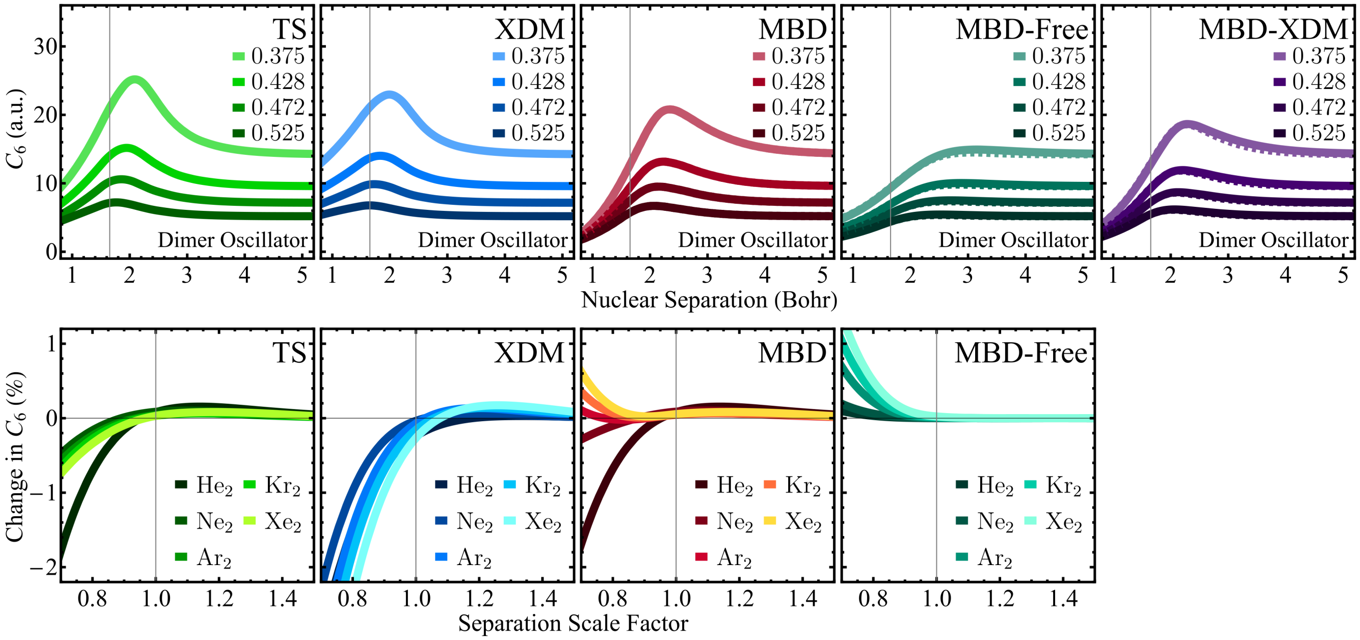

FIG. 7. Top: Effect of changing ω on C_6 on the dispersion corrections for the oscillator system's dimers. For the MBD methods, solid lines are C_6 coefficients derived from SCS polarizabilities and dashed lines are derived from rsSCS polarizabilities. Bottom: Variation in C_6 for noble-gas dimers with the internuclear separation ranging from 0.7× to 1.5× the reference equilibrium distance of the dimer.[111] Calculations were performed with FHI-aims for various dispersion models, using PBE with "tight" basis sets. For the MBD methods, the rsSCS routine was used. The vertical lines indicate the equilibrium bond distances for each system.

catastrophe", which is a known issue with self-consistent screening. MBD's SCS routine relies on Applequist's interactive dipole model which predicts the divergence of polarizabilities at low separation.[115] For chemical systems, the use of cutoffs or damping functions to address this issue is considered essential.[75]

The MBD model attempts to address the issue of excessive polarization by smearing interacting point dipoles into spherical Gaussian charge distributions via Eq. (30). This choice of interaction potential attenuates the polarizability to converge to a finite value at zero separation.[53] The rsSCS routine further damps the MBD energy at short range via a Wu-Yang damping function.[32] Despite these efforts, we see that MBD@rsSCS still suffers from unphysical polarizabilities. Focusing on Fig. 6's results for the central atom in the Ar trimer, MBD-Free exhibits a "polarization catastrophe", but not regular MBD. This again illustrates how sensitive the MBD method is to the starting point and indicates that modifications of MBD to avoid the (rs)SCS scheme[57] may provide some much-needed stability.

Further, despite the MBD and MBD-Free C_6 coefficients being reported at short-range in Fig. 5, at separations below the equilibrium bond length, MBD and MBD-Free typically generated complex-valued energies. This behaviour will be discussed further in Section 4.4 but, as a result, the short-range MBD results presented above should only be interpreted qualitatively.

4.3. Effect of Oscillator Frequency

For the oscillator models, the results shown so far have all used $\alpha^{\text{free}} = 9/2$ a.u. and the corresponding $\omega = 0.4715$ a.u. The oscillator frequency controls the spring constant for the interaction between the electron and nucleus, which then determines the oscillator polarizability. To investigate how the environmental/electronic many-body effects change with element, we performed additional calculations for the dimer model in which the oscillation frequency, ω, was systematically varied. The considered values of ω correspond to the various starting points discussed in Section 3.2. Additionally, $\omega = 0.525$ was also used to test a higher frequency, corresponding to a more strongly-bound electron. For each ω, the polarizability, α, was adjusted appropriately using Eq. (48).

The C_6 results for variable ω are shown in the top row of Fig. 7. For large frequencies, the electron is strongly bound to the oscillator (high excitation energy), resulting in low polarizability. Conversely, for low frequencies, the electron is weakly bound to the oscillator (low excitation energy), resulting in high polarizability. Therefore, we expect larger variability in C_6 with environment for more polarizable oscillators, corresponding to small ω. This is exactly what is seen in Fig. 7 for all methods, though, MBD-Free shows less dependence of C_6 on ω values than the other corrections.

To connect this result with real atomic systems, we also computed dispersion coefficients for the series of ho-

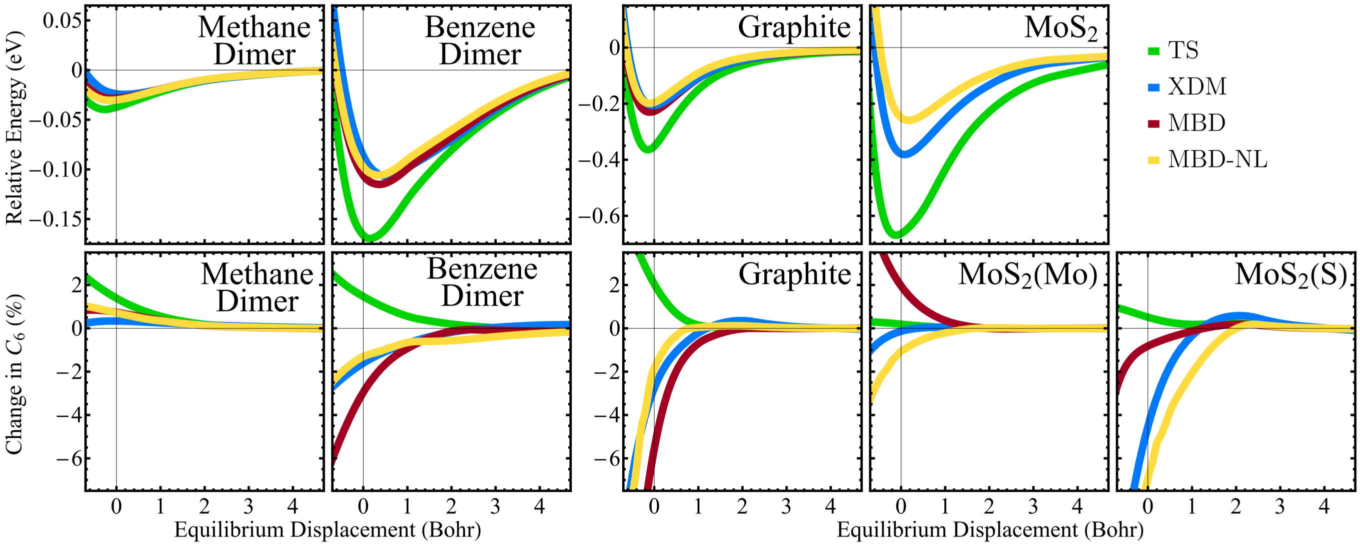

FIG. 8. The potential energy curves (top) and change in dispersion coefficients (bottom) for selected molecular dimers and layered materials, computed using the PBE functional, "light" basis sets and "dense" integration grids with FHI-aims. For MBD, the rsSCS routine was used. Evaluation of the MBD energies failed to converge for MoS_2, so those results are omitted. The vertical lines indicate the reference equilibrium separation for each system.[116,117]

moatomic noble-gas dimers from He_2 to Xe_2. The calculations were performed for the TS, XDM, MBD, and MBD-Free dispersion models with FHI-aims using the "tight" basis sets and the PBE density functional. The results are shown in the bottom row of Fig. 7. Since the noble gas atoms all have very strongly bound electrons (high ionization potentials), the results are similar to those obtained with the oscillators for the highest ω. There is only a modest increase in C_6 near the equilibrium separation, relative to the free-atom limit. XDM most clearly recovers the trend seen for the oscillators, with the variability in C_6 increasing with higher polarizability down the noble-gas group. Further, we note that only XDM predicts non-constant C_6 gradients near the equilibrium bond distance for both the oscillator and noble-gas systems, which has implications for the calculation of dispersion forces.[47] At short separations, the MBD and MBD-Free results again show a polarization catastrophe, with more rapid divergence of the dispersion coefficients occurring for more polarizable elements down the group. Notably, MBD only shows a polarization catastrophe for Ar_2, Kr_2, and Xe_2, while it occurs for all 5 noble gas dimers with MBD-Free.

4.4. Connection with Molecular Dimers and Layered Materials

To this point, we have seen that TS, XDM and MBD all give a consistent description of electronic many-body effects (i.e. changes in C_6 for varying atomic positions) in oscillator and atomic model systems. This stands in sharp contrast with previously observed behaviour for graphite.[27] In this section, we extend our comparison of various dispersion models to two molecular dimers (methane dimer and π-stacked benzene dimer in a parallel-displaced configuration) and two layered, solid-state materials (graphite and MoS_2).

The geometries of the molecular dimers were obtained from the S22×5 benchmark[116] and correspond to separations both at and away from equilibrium. The geometries of the periodic solids were obtained from Refs. 27,117 and the c lattice parameter systematically varied relative to the experimental reference value to consider expanded and compressed interlayer separations. Calculations using the PBE functional, "light" basis settings, "dense" integration grids, and each of the TS, XDM, MBD, and MBD-NL[57] dispersion methods, were performed with FHI-aims. For brevity, the @rsSCS label on MBD will be implied throughout in this section. For the layered materials, 12×12×4 **k**-point meshes were used. The resulting potential energy surfaces are shown in the top row of Fig. 8.

Note that the MBD-NL method represents yet another possible starting point for MBD.[57] In MBD@rsSCS, there is a related problem to the "polarization catastrophe" where some dipole interaction tensor elements become similar in magnitude to the inverse values of the polarizabilities when the starting polarizability is too high, typically occurring at small separations, or in ionic or metallic systems. This behaviour results in negative eigenvalues, suggesting that these induced dipoles are (unphysically) aligned anti-parallel to the applied field,[68] and leads to complex-valued energies via Eq. (34). A number of notable MBD variants that have been proposed to help with this problem include the fractionally-ionic variant[55] (MBD/FI), the use of iterative Hirshfeld partitioning[118,119] (MBD/HI), or the use of a polariz-

TABLE 1. Computed binding energies, in kcal/mol for the molecular dimers and in meV/Å^2 for the layered materials. Literature reference data[116,117] is shown for comparison. Also included are mean absolute errors (MAE) for the S66×8 benchmark[101] of molecular complexes and two benchmarks of layered materials.[117,122]

System	TS	MBD	MBD-NL	XDM	Ref.
$(CH_4)_2$	0.91	0.66	0.70	0.57	0.53
$(C_6H_6)_2$	3.91	2.65	2.44	2.46	2.81
Graphite	34.47	21.78	18.82	19.56	18.32
MoS_2	38.62	—	14.98	22.01	20.53
S66×8 (kcal/mol)	0.60	0.44	0.43	0.45	—
LM11 (meV/Å^2)	12.5	—	5.0	3.7	—
LM26 (meV/Å^2)	13.1	—	4.6	4.9	—

TABLE 2. Computed homoatomic C_6 dispersion coefficients, in a.u. for single isolated molecules and selected layered materials at large interlayer separation. The homoatomic free C_6 values for C, S,[65] and Mo,[68] were taken from available reference data. Also included are mean absolute percent errors (MAPE) and mean percent errors (MPE) for a set of 20 homomolecular C_6 dispersion coefficients (MolC_6).

System	Atom	Free	TS	MBD	MBD-NL	XDM
CH_4	C	46.6	26.0	31.7	27.6	18.7
C_6H_6	C	46.6	32.6	30.7	28.6	21.4
Graphite	C	46.6	35.4	33.3	27.7	20.2
MoS_2	Mo	1029	1060	627	260	388
MoS_2	S	134.0	132	80.3	101	78.5
MolC_6 MAPE (%)		–	12.7	13.1	7.3	20.1
MolC_6 MPE (%)		–	2.5	-3.2	-2.2	-18.2

ability functional[57] (MBD-NL). In MBD-NL, the initial polarizabilities and dispersion coefficients are taken from the non-local VV10 dispersion model.[120,121] Unlike other MBD variants, MBD-NL does not refine the polarizabilities with SCS, thus avoiding the polarization catastrophe. Instead, the VV10 polarizabilities are refined with cutoffs and used to obtain the characteristic excitation frequency via Eq. (28). The polarizabilities, characteristic excitation frequencies, and the damped long-range dipole potential of Eq. (37) are then used compute the MBD-NL energy via the matrix methods described in Section 2.5. This variant of MBD is recommended specifically for layered materials, such as the transition-metal dichalocogenides, where the rsSCS scheme cannot provide converged energies from the usual TS starting point.

With each method, homoatomic dispersion coefficients were evaluated at each point along the PES and their relative values are shown in Fig. 8 as a function of intermolecular or interlayer separation. The methane dimer, the parallel-displaced benzene dimer, and graphite results are all qualitatively similar. XDM and MBD show similar behaviour to each other, with an initial increase in C_6 as the molecules/layers approach each other, followed by a sharp decrease. Again, this is similar to the results of these methods for the oscillator models and noble-gas systems. The outlier is the TS method, which shows starkly different behaviour for the molecular dimers and graphite than seen above for the oscillators and noble gases. Specifically, TS shows a sharp increase in C_6 at small separations. It is not immediately clear why TS gives such different behaviour for molecules than for atomic dimers or chains; the increased Hirshfeld volumes upon compression may perhaps be due to the presence of covalently bonded atoms or the greater contact area between the interacting molecules/layers.

For MoS_2, only XDM and MBD-NL predict similar changes in C_6 with interlayer separation for both bulk materials. Here, the MBD method strongly over polarizes and the Mo dispersion coefficients sharply increase for separations near the equilibrium displacement. This is because the TS starting point gives very high initial C_6 coefficients and polarizabilities for the Mo atoms, as we will see. Conversely, MBD-NL is well behaved due to having a much lower input polarizability and avoiding the SCS routine, therefore avoiding these polarization issues for MoS_2 and showing a decrease in C_6 at short separations similar to XDM. We note, however, that MBD-NL exhibits small oscillations in its C_6 dispersion coefficients' curves in Fig. 8, suggesting that there may be some numerical instability.

To quantitatively assess the quality of the PES, the computed binding energies are compared with high-level reference data in Table 1. The XDM, MBD, and MBD-NL results are generally in fairly close agreement, while TS strongly overbinds. The greatest spread between the methods occurs for MoS_2. To provide a better statistical comparison, we also report mean absolute errors (MAEs) obtained with the same collection of methods for the binding energies of the S66×8 set of molecular complexes[101] and the exfoliation energies of Bojrkman's LM26 set[117] (and its smaller LM11 subset considered by Tawfik *et al.*[122]) of layered materials in Table 1. These benchmarks were computed in FHI-aims using the PBE base functional, "light" basis settings, and "dense" integration grids. Again, for layered materials, 12×12×4 **k**-point meshes were used throughout. MBD, MBD-NL, and XDM all give comparable performance for the S66×8 benchmark when paired with the PBE base functional. The interested reader is directed to Ref. 113 for the results with differing functionals and with the "tight" basis settings. No MBD result is given for the layered benchmark since the MBD energy evaluation consistently predicted complex-valued energies for transition metal dichalcogenides. Here, TS massively overbinds, similar to what was seen for the specific case of MoS_2, while MBD-NL and XDM again give comparable, good performance.

To evaluate the accuracy of the various methods for homomolecular C_6 dispersion coefficients, we constructed a C_6 benchmark using a set of 20 molecules: H_2, N_2, O_2, Cl_2, CO_2, methane, CCl_4, SiH_4, SiF_4, SF_6, ethyne, ethene, ethane, propene, propane, butene, butane, pentane, hexane, and benzene. Reference data was collected from Ref. 123, and computations were performed using FHI-aims with the PBE functional and "tight" basis settings. During the initial development of XDM, it was found to give a mean (absolute) percent error of only 0.3% (3.4%) for the C_6 dispersion coefficients of all combinations of H, He, Ne, Ar, Kr, and Xe.[29] Conversely, for this set of 20 molecules, the results in Table 2 show that XDM systematically underestimates the homomolecular C_6 dispersion coefficients, while TS, MBD, and MBD-NL give mean percent errors much closer to zero. The systematic underestimation of molecular C_6 dispersion coefficients with XDM, despite its excellent performance for isolated atoms, is likely because of its use of simplistic volume scaling to obtain isotropic atomic polarizabilities. Similar to how MBD likely relies on its damping function to compensate for missing C_8 and higher-order dispersion terms, XDM likely relies on its damping function to compensate for underestimation of C_6.

Finally, selected homoatomic dispersion coefficients for the non-hydrogen atoms in methane, benzene, graphite, and MoS_2 are collected in Table 2 and show much larger differences between methods than were seen for the benchmark of 20 homomolecular C_6 coefficients. Particularly for MoS_2, the chemical bonding causes large changes in C_6 relative to the free-atomic values, as noted previously.[27] The coefficients follow the general trend of Free > TS ≈ MBD > MBD-NL > XDM for C, and Free ≈ TS > MBD > MBD-NL ≈ XDM for S and Mo, which explains the trends in MoS_2 exfoliation energies in Table 1. While there is no reference data for accurate C_6 coefficients of Mo and S in MoS_2, the XDM and MBD-NL values would be expected to be the most reliable estimates given the good performance of these two methods for the exfoliation energy benchmarks (Table 1).

CONCLUSION

In this work, we constructed and variationally optimized wavefunctions for a series of model systems composed of interacting quantum harmonic oscillators. From these wavefunctions, we evaluated dispersion coefficients and energies with the XDM, TS, and several variants of the MBD dispersion methods. The results showed a significant difference in dispersion energies between XDM, which includes higher-order C_8 and C_{10} contributions, and the TS and MBD methods that do not. Conversely, when considering the damped dispersion energies, all give nearly identical results at long range and, at intermediate range, MBD is in excellent agreement with a reparameterized version of XDM that uses only the C_6 term.

Turning to the dispersion coefficients, the rsSCS modification of MBD seems to provide a stabilizing effect, reducing the variation of the dispersion coefficients with surrounding environment. All the dispersion models considered showed similar behaviour for the variation in C_6 with nuclear separation, although the MBD-based methods showed evidence of a "polarization catastrophe" at short distances. Qualitatively similar results to those for the quantum harmonic oscillators were obtained for dimers, trimers, and tetramers of Ar atoms, with the MBD-based methods again exhibiting a polarization catastrophe at short internuclear separations. We additionally investigated how the dispersion coefficients of two interacting oscillators change with their vibrational frequency. In general, we found greater variations in C_6 with surrounding environment (i.e. the distance between the coupled oscillators) for lower vibrational frequencies, which corresponds to higher polarizability. Similar behaviour was observed for DFT calculations on noble gas dimers, where the polarizability increases down the group.

Finally, we performed calculations on the homomolecular dimers of methane and benzene, as well as graphite and MoS_2 to determine if the results obtained for the oscillators and noble gases were transferable to larger chemical systems. Overall, we found similar dependence of the dispersion coefficients on centre-of-mass or interlayer separation. The exception to this was the TS method, where the dispersion coefficients would increase sharply at small distances, resembling the polarization catastrophe, but occurring due to increases in the Hirshfeld atomic volumes. This behaviour would appear to make the TS dispersion coefficients and polarizabilities a less-than-optimal starting point for the MBD method.

A key finding of this work is that the SCS/rsSCS schemes used in MBD show a concerning sensitivity to the choice of input polarizabilities and dispersion coefficients. While a TS starting point is the usual choice, this is by no means the only option and it can result in unphysical polarizabilities, and generating complex-valued energies in cases like MoS_2. This occurs because TS gives dispersion coefficients and polarizabilities that are similar to, or higher than, the free-atom values for Mo atoms for the bulk solid. The NL variant of MBD, which is recommended for layered materials and metals, avoids these polarization issues, and is suitable for all chemical systems considered in this work. We therefore recommend MBD-NL over MBD@rsSCS generally. Perhaps the VV10 polarizability functional used in MBD-NL could also be integrated into the XDM to improve the model's treatment of dynamic dipole polarizability. Indeed, this could be an interesting avenue to explore in a future study.

The original purpose of this work was to compare and contrast the different dispersion corrections to understand how each accounted for electronic and atomic many-body effects. Our results show that TS, XDM, and MBD all exhibit roughly the same magnitude of variation in C_6 with changing environment for weak interactions between oscillators or noble gases, demonstrating that they all capture electronic many-body effects for these systems. The agreement of TS with XDM-C_6 and MBD for undamped and damped dispersion energies of the oscillator model systems, when it shows very different behaviour for molecules and materials, limits our ability to draw further conclusions.

For the oscillator model systems, we see that XDM-

C_6 and MBD@rsSCS (when parameterized similarly) give effectively identical damped dispersion energies for both intermediate- and long-range interactions. Further, MBD's 3-body energy contribution, computed via the ACFD-RPA correlation energy, is in near perfect agreement with the ATM energy calculated via XDM. In both cases, these 3-body energy contributions proved to be negligible for the model oscillator systems, although MBD's 3-body contributions are reported to become significant for some supermolecular complexes and biochemical systems.[33] These results suggest that it would be of pedagogical interest to study these 3-body contributions for larger systems. For now, this further confirms our previous conclusion[21] that electronic many-body effects and the inclusion of higher-order, pairwise dispersion energies represent far more important contributions to the physics of London dispersion than the triple-dipole ATM term. Overall, our findings suggest that quantum harmonic oscillators may be too simple a model system to assess the performance of dispersion models, since they are missing many of the intricacies of dispersion interactions in molecular and solid-state systems.

ACKNOWLEDGEMENTS

This research was funded by the Natural Sciences and Engineering Research Council of Canada (NSERC). The authors are grateful to ACENET and Digital Research Alliance of Canada for computational resources. We also thank the Killam Trust and the Walter C. Sumner Foundation for fellowships to KRB.

DATA AVAILABILITY STATEMENT

The data and Mathematica code that support this study are openly available from GitHub at `https://github.com/KyleBryenton/Oscillators_2023`.[124]

CONFLICT OF INTEREST

The authors have declared no conflicts of interest for this article.

ORCID

Kyle R. Bryenton
`https://orcid.org/0000-0001-5716-5314`
Erin R. Johnson
`https://orcid.org/0000-0002-5651-468X`

REFERENCES

[1] F. London, Z. Phys. **63**, 245 (1930).
[2] F. London, Trans. Faraday Soc. **33**, 8b (1937).
[3] J. D. van der Waals, Leiden University, Leiden, Netherlands , 301 (1873).
[4] K. Autumn, M. Sitti, Y. A. Liang, A. M. Peattie, W. R. Hansen, S. Sponberg, T. W. Kenny, R. Fearing, J. N. Israelachvili, and R. J. Full, Proc. Natl. Acad. Sci. **99**, 12252 (2002).
[5] M. Lessel, P. Loskill, F. Hausen, N. N. Gosvami, R. Bennewitz, and K. Jacobs, Phys. Rev. Lett. **111**, 035502 (2013).
[6] W. Liu, A. Tkatchenko, and M. Scheffler, Acc. Chem. Res. **47**, 3369 (2014).
[7] M. Micoulaut, A. Piarristeguy, H. Flores-Ruiz, and A. Pradel, Phys. Rev. B **96**, 184204 (2017).
[8] T. Risthaus and S. Grimme, J. Chem. Theory Comput. **9**, 1580 (2013).
[9] J. Moellmann and S. Grimme, Phys. Chem. Chem. Phys. **12**, 8500 (2010).
[10] M. Kolář, T. Kubař, and P. Hobza, J. Phys. Chem. B **115**, 8038 (2011).
[11] A. Tkatchenko, R. A. DiStasio Jr, R. Car, and M. Scheffler, Phys. Rev. Lett. **108**, 236402 (2012).
[12] A. Ambrosetti, D. Alfè, R. A. DiStasio Jr, and A. Tkatchenko, J. Phys. Chem. Lett. **5**, 849 (2014).
[13] A. M. Reilly and A. Tkatchenko, J. Chem. Phys. **139**, 024705 (2013).
[14] W. Ouyang, I. Azuri, D. Mandelli, A. Tkatchenko, L. Kronik, M. Urbakh, and O. Hod, J. Chem. Theory Comput. **16**, 666 (2019).
[15] F. Maass, M. Ajdari, F. C. Kabeer, M. Vogtland, A. Tkatchenko, and P. Tegeder, J. Phys. Chem. Lett. **10**, 1000 (2019).
[16] M. Stöhr and A. Tkatchenko, Sci. Adv. **5**, eaax0024 (2019).
[17] F. Schubert, M. Rossi, C. Baldauf, K. Pagel, S. Warnke, G. von Helden, F. Filsinger, P. Kupser, G. Meijer, M. Salwiczek, *et al.*, Phys. Chem. Chem. Phys. **17**, 7373 (2015).
[18] V. V. Gobre and A. Tkatchenko, Nat. Commun. **4**, 1 (2013).
[19] A. M. Reilly and A. Tkatchenko, Phys. Rev. Lett. **113**, 055701 (2014).
[20] A. M. Reilly and A. Tkatchenko, Chem. Sci. **6**, 3289 (2015).
[21] A. Otero-de-la-Roza, L. M. LeBlanc, and E. R. Johnson, Phys. Chem. Chem. Phys. **22**, 8266 (2020).
[22] B. Axilrod and E. Teller, J. Chem. Phys. **11**, 299 (1943).
[23] Y. Muto, J. Phys. Math. Soc. Japan **17**, 629 (1943).
[24] J. F. Dobson, Int. J. Quantum Chem. **114**, 1157 (2014).
[25] A. Otero-de-la-Roza and E. R. Johnson, J. Chem. Phys. **138**, 054103 (2013).
[26] E. R. Johnson, J. Chem. Phys. **135**, 234109 (2011).
[27] A. Otero-de-la-Roza, L. M. LeBlanc, and E. R. John-

son, J. Phys. Chem. Lett. **11**, 2298 (2020).
[28]E. R. Johnson and A. D. Becke, J. Chem. Phys. **124**, 174104 (2006).
[29]A. D. Becke and E. R. Johnson, J. Chem. Phys. **127**, 154108 (2007).
[30]A. Otero-de-la-Roza and E. R. Johnson, J. Chem. Phys. **136**, 174109 (2012).
[31]E. R. Johnson, "The exchange-hole dipole moment dispersion model," in *Non-covalent Interactions in Quantum Chemistry and Physics: Theory and Applications* (Elsevier, 2017) Chap. 5, pp. 169–194, edited by Alberto Otero de la Roza and Gino A DiLabio.
[32]A. Ambrosetti, A. M. Reilly, R. A. DiStasio Jr, and A. Tkatchenko, J. Chem. Phys. **140**, 18A508 (2014).
[33]R. A. DiStasio Jr, O. A. von Lilienfeld, and A. Tkatchenko, Proc. Nat. Acad. Sci. **109**, 14791 (2012).
[34]A. Tkatchenko, A. Ambrosetti, and R. A. DiStasio Jr, J. Chem. Phys. **138**, 074106 (2013).
[35]J. Hermann, R. A. DiStasio Jr, and A. Tkatchenko, Chem. Rev. **117**, 4714 (2017).
[36]A. Tkatchenko and M. Scheffler, Phys. Rev. Lett. **102**, 073005 (2009).
[37]A. Ambrosetti, N. Ferri, R. A. DiStasio Jr, and A. Tkatchenko, Science **351**, 1171 (2016).
[38]P. Hohenberg and W. Kohn, Phys. Rev. **136**, B864 (1964).
[39]W. Kohn and L. J. Sham, Phys. Rev. **140**, A1133 (1965).
[40]K. Burke, J. Chem. Phys. **136**, 150901 (2012).
[41]A. D. Becke, J. Chem. Phys. **140**, 18A301 (2014).
[42]S. Kristyán and P. Pulay, Chem. Phys. Lett. **229**, 175 (1994).
[43]J. Pérez-Jordá and A. D. Becke, Chem. Phys. Lett. **233**, 134 (1995).
[44]P. Hobza, J. šponer, and T. Reschel, J. Comput. Chem. **16**, 1315 (1995).
[45]E. R. Johnson, R. A. Wolkow, and G. A. DiLabio, Chem. Phys. Lett. **394**, 334 (2004).
[46]S. Grimme, WIREs Comput. Mol. Sci. **1**, 211 (2011).
[47]A. J. A. Price, K. R. Bryenton, and E. R. Johnson, J. Chem. Phys. **154**, 230902 (2021).
[48]S. Grimme, J. Comput. Chem. **25**, 1463 (2004).
[49]S. Grimme, J. Comput. Chem. **27**, 1787 (2006).
[50]S. Grimme, J. Antony, S. Ehrlich, and H. Krieg, J. Chem. Phys. **132**, 154104 (2010).
[51]E. Caldeweyher, S. Ehlert, A. Hansen, H. Neugebauer, S. Spicher, C. Bannwarth, and S. Grimme, J. Chem. Phys. **150**, 154122 (2019).
[52]E. Caldeweyher, J.-M. Mewes, S. Ehlert, and S. Grimme, Phys. Chem. Chem. Phys. **22**, 8499 (2020).
[53]R. A. DiStasio, V. V. Gobre, and A. Tkatchenko, J. Phys.: Condens. Matter **26**, 213202 (2014).
[54]V. G. Ruiz, W. Liu, and A. Tkatchenko, Phys. Rev. B **93**, 035118 (2016).
[55]T. Gould, S. Lebègue, J. G. Ángyán, and T. Bučko, J. Chem. Theory Comput. **12**, 5920 (2016).
[56]M. Kim, W. J. Kim, T. Gould, E. K. Lee, S. Lebègue, and H. Kim, J. Am. Chem. Soc. **142**, 2346 (2020).
[57]J. Hermann and A. Tkatchenko, Phys. Rev. Lett. **124**, 146401 (2020).
[58]F. O. Kannemann and A. D. Becke, J. Chem. Theory Comput. **6**, 1081 (2010).
[59]A. Otero-de-la-Roza and E. R. Johnson, J. Chem. Phys. **138**, 204109 (2013).
[60]A. D. Becke and M. R. Roussel, Phys. Rev. A **39**, 3761 (1989).
[61]A. D. Becke and E. R. Johnson, J. Chem. Phys. **127**, 124108 (2007).
[62]J. R. Rumble, *CRC handbook of chemistry and physics*, Vol. 102 (CRC press, 2021).
[63]A. Otero-de-la-Roza, G. A. DiLabio, and E. R. Johnson, J. Chem. Theory Comput. **12**, 3160 (2016).
[64]Q. Wu and W. Yang, J. Chem. Phys. **116**, 515 (2002).
[65]X. Chu and A. Dalgarno, J. Chem. Phys. **121**, 4083 (2004).
[66]J. a. Mitroy, M. S. Safronova, and C. W. Clark, J. Phys. B: At. Mol. Opt. Phys. **43**, 202001 (2010).
[67]V. Dzuba, A. Kozlov, and V. Flambaum, Phys. Rev. A **89**, 042507 (2014).
[68]V. V. Gobre, *Efficient modelling of linear electronic polarization in materials using atomic response functions*, Ph.D. thesis, Technische Universitaet Berlin, Straße des 17. Juni 135, 10623 Berlin, Germany (2016).
[69]J. C. Slater and J. G. Kirkwood, Phys. Rev. **37**, 682 (1931).
[70]C. Mavroyannis and M. J. Stephen, Mol. Phys. **5**, 629 (1962).
[71]K. T. Tang, Phys. Rev. **177**, 108 (1969).
[72]A. Stone, *The Theory of Intermolecular Forces*, 2nd ed. (Oxford University Press, 2013).
[73]B. U. Felderhof, Physica **76**, 486 (1974).
[74]D. W. Oxtoby and W. M. Gelbart, Mol. Phys. **29**, 1569 (1975).
[75]B. T. Thole, Chem. Phys. **59**, 341 (1981).
[76]H. Padé, in *Scientific annals of the école Normale Supérieure*, Vol. 9 (1892) pp. 3–93.
[77]G. A. Baker Jr, "The theory and application of the padé approximant method," Tech. Rep. (Los Alamos Scientific Lab., Univ. of California, N. Mex., 1964).
[78]K. T. Tang and M. Karplus, Phys. Rev. **171**, 70 (1968).
[79]W. W. Bell, *Special functions for scientists and engineers* (Courier Corporation, 2004).
[80]J. W. L. Glaisher, London, Edinburgh, and Dublin Philos. Mag. and J. Sci. **42**, 294 (1871).
[81]H. B. G. Casimir and D. Polder, Phys. Rev. **73**, 360 (1948).
[82]A. Lucas, Physica **35**, 353 (1967).
[83]A. G. Donchev, J. Chem. Phys. **125**, 074713 (2006).
[84]J. Cao and B. J. Berne, J. Chem. Phys. **97**, 8628 (1992).
[85]M. W. Cole, D. Velegol, H.-Y. Kim, and A. A. Lucas, Mol. Simul. **35**, 849 (2009).

[86]H. Berthoumieux and A. C. Maggs, Europhys. Lett. **91**, 56006 (2010).
[87]W. L. Bade, J. Chem. Phys. **27**, 1280 (1957).
[88]W. Bade and J. G. Kirkwood, J. Chem. Phys. **27**, 1284 (1957).
[89]Eq. (33) requires α_i^{SCS} and ω_i^{SCS} to be independent of frequency, as indicated within `mbd_methods.f90` in the FHI-aims code, retrieved 2022/12.
[90]D. Massa, A. Ambrosetti, and P. L. Silvestrelli, J. Chem. Phys. **154**, 224115 (2021).
[91]P. P. Poier, O. Adjoua, L. Lagardère, and J.-P. Piquemal, J. Phys. Chem. Lett. **14**, 1609 (2023).
[92]D. C. Langreth and J. P. Perdew, Solid State Commun. **17**, 1425 (1975).
[93]D. C. Langreth and J. P. Perdew, Phys. Rev. B **15**, 2884 (1977).
[94]O. Gunnarsson and B. I. Lundqvist, Phys. Rev. B **13**, 4274 (1976).
[95]O. Gunnarsson and B. Lundqvist, Phys. Rev. B **15**, 6006 (1977).
[96]D. Bohm and D. Pines, Phys. Rev. **92**, 609 (1953).
[97]M. Gell-Mann and K. A. Brueckner, Phys. Rev. **106**, 364 (1957).
[98]P. Jurečka, J. Šponer, J. Černỳ, and P. Hobza, Phys. Chem. Chem. Phys. **8**, 1985 (2006).
[99]J. Rezác, K. E. Riley, and P. Hobza, J. Chem. Theory Comput. **7**, 2427 (2011).
[100]J. Rezác, K. E. Riley, and P. Hobza, J. Chem. Theory Comput. **10**, 1359 (2014).
[101]B. Brauer, M. K. Kesharwani, S. Kozuch, and J. M. Martin, Phys. Chem. Chem. Phys. **18**, 20905 (2016).
[102]J. Claudot, W. J. Kim, A. Dixit, H. Kim, T. Gould, D. Rocca, and S. Lebègue, J. Chem. Phys. **148**, 064112 (2018).
[103]A. Messiah, *Quantum mechanicstwo volumes bound as one* (Dover Publications New York, 2000).
[104]M. Born and R. Oppenheimer, Ann. Phys. **389**, 457 (1927).
[105]W. Kauzmann, *Quantum chemistry: an introduction* (Elsevier, 2013).
[106]J. Stewart, D. K. Clegg, and S. Watson, *Calculus: early transcendentals* (Cengage Learning, 2020) pp. 971–981.
[107]F. O. Kannemann, *Development and benchmarking of a semilocal density-functional approximation including dispersion*, Ph.D. thesis, Department of Chemistry, Dalhousie University, Halifax, Nova Scotia, Canada (2013).
[108]J. P. Perdew and W. Yue, Phys. Rev. B **33**, 8800 (1986).
[109]J. P. Perdew, K. Burke, and M. Ernzerhof, Phys. Rev. Lett. **77**, 3865 (1996).
[110]S. F. Boys and F. Bernardi, Mol. Phys. **19**, 553 (1970).
[111]K. Tang and J. Toennies, J. Chem. Phys. **118**, 4976 (2003).
[112]V. Blum, R. Gehrke, F. Hanke, P. Havu, V. Havu, X. Ren, K. Reuter, and M. Scheffler, Comput. Phys. Commun. **180**, 2175 (2009).
[113]A. J. Price, A. Otero-de-la Roza, and E. R. Johnson, Chem. Sci. (2023), 10.1039/D2SC05997E.
[114]A. D. Becke, J. Chem. Phys. **85**, 7184 (1986).
[115]J. Applequist, J. R. Carl, and K.-K. Fung, J. Am. Chem. Soc **94**, 2952 (1972).
[116]L. Gráfová, M. Pitonak, J. Rezac, and P. Hobza, J. Chem. Theory Comput. **6**, 2365 (2010).
[117]T. Björkman, J. Chem. Phys. **141**, 074708 (2014).
[118]T. Bučko, S. Lebègue, J. Hafner, and J. G. Ángyán, J. Chem. Theory Comput. **9**, 4293 (2013).
[119]T. Bučko, S. Lebègue, J. G. Ángyán, and J. Hafner, J. Chem. Phys. **141**, 034114 (2014).
[120]O. A. Vydrov and T. Van Voorhis, J. Chem. Phys. **133**, 244103 (2010).
[121]O. A. Vydrov and T. Van Voorhis, Phys. Rev. A **81**, 062708 (2010).
[122]S. A. Tawfik, T. Gould, C. Stampfl, and M. J. Ford, Phys. Rev. Mater. **2**, 034005 (2018).
[123]E. R. Johnson and A. D. Becke, J. Chem. Phys. **123**, 024101 (2005).
[124]K. R. Bryenton, "Kylebryenton/oscillators_2023: 2023-05-01," (2023).